Hydrodynamic Pressure Field Caused by a Ship Sailing Near the Coast

Authors: Deng, Hui, Zhang, Zhi-hong, Gu, Jian-nong, and Liu, Ju-bin

Hydrodynamic Pressure Field Caused by a Ship Sailing Near the Coast

Hui Deng, Zhi-hong Zhang*, Jian-nong Gu, and Ju-bin Liu

College of Science
Naval University of Engineering
Wuhan 430033, China

www.cerf-jcr.org

www.JCRonline.org

ABSTRACT

Deng, H.; Zhang, Z.-H.; Gu, J.-N., and Liu, J.-B., 2016. Hydrodynamic pressure field caused by a ship sailing near the coast. *Journal of Coastal Research,* 32(4), 890–897. Coconut Creek (Florida), ISSN 0749-0208.

Based on the shallow-water wave-potential flow theory and the assumption of a slender ship, a mathematical model, whose dispersion relation is improved, has been established for the ship hydrodynamic pressure field (SHPF), which is suitable for a wider speed range. The finite difference method is used for calculating the SHPF, and the artificial viscous terms are added in the boundary conditions to ensure the stability of the nonlinear equation solution. The comparison between the calculated results and the experimental ones shows that the calculation method is feasible and the improved mathematical model is more accurate and effective. The calculation and analysis of the SHPF caused by ships deviating from the channel centre line or sailing near the coast in shallow water indicate that the narrower the distance between the ship and the coastal sidewall the greater will its effects be on the coast, the seabed, and the coastal architecture around the ship at the subcritical speed, which will cause effects on the coast, seabed, and coastal architectures of a wider water area behind the ship to a large extent at supercritical speed.

ADDITIONAL INDEX WORDS: *Ship hydrodynamic pressure field, ship motion, coast, safe navigation, coastal destruction.*

INTRODUCTION

When a ship moves, there is pressure variation in the flow field, and the pressure variation caused by a moving ship is called the ship hydrodynamic pressure field (SHPF). In recent years, with the development of shipping, there are more ships moving in shallow water, such as coastal waters and channels. In shallow water or near the coast, the SHPF may affect the coast and the seabed and lead to instability of the coastal architecture; accordingly, the wave–current interaction, the coast, and the seabed may make changes to the ship's wetted surface area and affect its safe navigation (Zheng and Li, 2015; Zheng *et al*., 2014). Meanwhile, because pressure variation caused by a moving ship is distinct from that caused by the movement of other ships, the signal characteristic of the SHPF is often used to discover and identify a ship. Since 1960, many experts and scholars have focused attention on safe navigation and coastal environment hydrodynamics pressure fields. The SHPF caused by a slender ship moving at low speed in shallow water had been analyzed (Tuck, 1966, 1978, 1998), as has theoretical modelling and numerical computation of SHPF caused by submarines, surface ships, and hovercrafts, using the Green function method of finite-depth water (Sahin, Crane, and Watson, 1997; Sahin and Hyman, 1993; Sahin, Hyman, and Nguyen, 1994). A series of articles concerning experimental SHPF in tanks and the ocean were published, and the effects of ship type, propeller, and flow on SHPF were analyzed in

the theoretical research (Kozaczka and Milanowski, 1997; Kozaczka and Milanowski, 1995a,b; Kozaczka *et al*., 1996). A series of analytic solutions for SHPF in open waters, without considering nonlinear and dispersive effects, has been obtained (Zhang and Gu, 2006; Zhang *et al*., 2002a,b). The distribution of pressure induced by a ship moving in finite-depth water has been calculated using the panel method (Li *et al*., 2011; Miao, Zhang, and Gu, 2012). The SHPF caused by a ship moving along the channel centre line at subcritical and supercritical speeds in shallow water was calculated with the finite-difference method (Deng *et al*., 2014, 2013). However, most of the studies mentioned were aimed at ships moving along the channel centre line or in open waters, but during an actual voyage, ships often deviate from the channel centre line or sail near the coast, with the distance between the ship and the coast changing, which means the SHPF will also change. At present, the theoretical models and numerical calculations for shallow-water SHPF are not sufficient for practical applications. Basis on our previous research (Deng *et al*., 2013, 2014), in this article, we deduced a theoretical model with improved dispersion relation, which will yield better results at a wider speed range. Primarily, we performed numerical calculations on the hydrodynamic pressure caused by a ship deviating from the channel centre line or sailing near the coast, through which, a more-accurate picture of SHPF and its influence on the coast can be obtained.

METHODS

First, we establish the SHPF theoretical model, and then we use numerical calculations to obtain the SHPF characteristics

*Corresponding author: zhangzhihong_999@163.com

caused by a ship deviating from the channel centre line or sailing near the coast.

Theoretical Model

As shown in Figure 1, a Cartesian coordinate system moving at the same speed as the ship is used, with the origin (O) located at the centre of the hull at the waterline, the x-axis pointing the direction of the ship motion, the y-axis pointing to the channel left sidewall, and the z-axis representing the vertical up. Suppose the ship length is L, its constant speed is V and the depth of the water is h. When the depth of water is less than $0.3L$ (Zhou and Zhen, 2006), it can be as a shallow-water area. When the ship moves with a constant speed in the water, the flow is relatively static, and it can be assumed to be inviscid, incompressible according to Helmholtz theorem, and irrotational, so the disturbance velocity potential Φ caused by the moving ship should meet the extended Kadomtsev–Petviashvili (KP) equation of constant depth in the shallow water, based on the related reference documents (Deng *et al*., 2013, 2014).

$$\begin{aligned} &\frac{2F_h}{\sqrt{gh}}\Phi_{xt} + (1-F_h^2)\Phi_{xx} + \Phi_{yy} + \frac{F_h^2 h^2}{3}\Phi_{xxxx} \\ &+ \frac{F_h^2 h^2}{3}\Phi_{xxyy} \frac{3F_h}{\sqrt{gh}}\Phi_x\Phi_{xx} + \frac{2F_h}{\sqrt{gh}}\Phi_{xy}\Phi_y + \frac{F_h}{\sqrt{gh}}\Phi_x\Phi_{yy} \\ &= 0 \end{aligned} \quad (1)$$

where Φ_x expresses a derivative of Φ for x, Φ_{xx} expresses a second derivative of Φ for x, and so on; F_h is the depth Froude number, an important characteristic parameter in marine dynamics, where $F_h < 1$ and $F_h > 1$ are known as subcritical and supercritical speed, respectively, and $F_h = 1$ denotes critical speed; $0.8 < F_h < 1.2$ is also referred to as the transcritical speed.

From experiments, we have found that when a ship moves at transcritical speed, the variation of waves in y-direction is weaker than it is in the x-direction, therefore, Equation (1) can be simplified to a standard KP equation:

$$\frac{2F_h}{\sqrt{gh}}\Phi_{xt} + (1-F_h^2)\Phi_{xx} + \Phi_{yy} + \frac{3V}{gh}\Phi_x\Phi_{xx} + \frac{F_h^2 h^2}{3}\Phi_{xxxx} = 0 \quad (2)$$

where Φ_{xt} expresses the unsteadiness, $\Phi_x\Phi_{xx}$ is the nonlinear effect, and Φ_{xxxx} is the dispersive effect.

Because the term for unsteadiness caused by a solitary wave exists only at a near-critical ($F_h \to 1$) speed, at other speeds, the unsteady term $[\Phi_{xt} = (\partial\Phi/\partial x\partial t) \to 0]$ can be ignored. Equation (2) can be reduced to a steady shallow-water wave equation that satisfies the Laplace equation, the free-surface conditions, and the seabed boundary conditions:

$$(1-F_h^2)\Phi_{xx} + \Phi_{yy} + \frac{3V}{gh}\Phi_x\Phi_{xx} + \frac{F_h^2 h^2}{3}\Phi_{xxxx} = 0 \quad (3)$$

To extend the applicable speed range of Equation (3), which would make it not only suitable for transcritical speed but also for subcritical or supercritical speed, the dispersion relation of Equation (3) was studied. We compared the dispersion relation of the linear wave theory to that of Equation (3), and the parameter β was added to the coefficient of the dispersive term Φ_{xxxx}, to improve the dispersion relation of Equation (3) and to
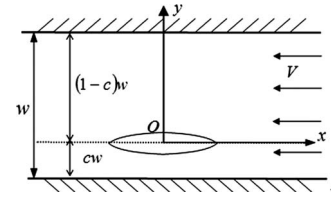

Figure 1. Coordinate system of theoretical model.

obtain a more-accurate backward position of $|C_{p_{\min}}|$ of SHPF in subcritical or supercritical speeds:

$$(1-F_h^2)\Phi_{xx} + \Phi_{yy} + \frac{3V}{gh}\Phi_x\Phi_{xx} + \left(\frac{1}{3}+\beta\right)F_h^2 h^2\Phi_{xxxx} = 0 \quad (4)$$

The improved KP equation (Equation 4), with the suitable parameter β, will yield a very good dispersion relation for a wider range of speeds. By setting the general solution of Equation (4) to a free-wave model, *i.e.* $\Phi \sim \exp(ik_x x + ik_y y)$, where k_x is $k\cos\theta$, k_y is $k\sin\theta$, k is the wave number, and θ is the direction of the wave propagation measured from x-direction. The approximate dispersion relation of Equation (3) can be obtained by substituting the solution into Equation (3).

$$F_h^2\cos^2\theta = \frac{1}{1+\frac{1}{3}\cos^2\theta\mu^2 k^2} \quad (5)$$

where $\mu = h/L$ is a small parameter.

The approximate dispersion relation of Equation (4) can also be obtained:

$$F_h^2\cos^2\theta = \frac{1}{1+\left(\frac{1}{3}+\beta\right)\cos^2\theta\mu^2 k^2} \quad (6)$$

The exact dispersion relation of the linear wave theory in finite-depth water uses the following form, and its right side can be expanded for a small μk:

$$F_h^2\cos^2\theta = \frac{\tanh\mu k}{\mu k} = \left(1 + \frac{\mu^2 k^2}{3} - \frac{\mu^4 k^4}{45} + \frac{2\mu^6 k^6}{945} - \cdots\right)^{-1} \quad (7)$$

Under steady conditions, the parameter β can be obtained by comparing the dispersion relation Equations (6) and (7):

$$\beta = \frac{1}{3}\tan^2\theta - \frac{\mu^2 k^2}{45\cos^2\theta} + \frac{2\mu^4 k^4}{945\cos^2\theta} \quad (8)$$

where μk and θ are relative to F_h. For a ship moving at subcritical speed, μk and θ can be obtained by calculating the empirical equation $F_h = \sqrt{\{\tanh\mu k[(3-2\mu k)/(\sinh 2\mu k)]\}/2\mu k}$ and Equation (7) (Jiang, 2001). As shown in Figure 2, when $F_h \to 0$, $\mu k \to \infty$, μk is not small and is much larger than 1, it can be not considered a shallow-water wave, so Equation (8) is not suitable for low subcritical speeds.

For a ship moving at supercritical speed, μk and θ can be obtained by calculating the theoretical equation $\theta = \arccos(1/F_h)$ and Equation (7) (Zhang, 2003).

Most high-speed ships are slender, so the slender-body theory can be used for setting the hull boundary condition:
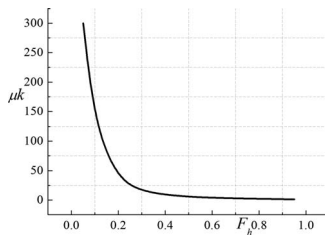
Figure 2. The wave number μk versus the Froude number F_h. Figure 2 helps us to determine the subcritical applicable scope of our equations. For example, when $F_h \to 0$, $\mu k \to \infty$, the μk is much larger than 1, so the wave can be not considered a shallow-water wave; therefore, our equations are not suitable for $F_h \to 0$.

$$\Phi_y = \mp \frac{VS_x(x)}{2h} \quad \text{as } |x| \le \frac{L}{2} \quad \text{and} \quad y = 0 \qquad (9)$$

where $S(x)$ is the cross-sectional area under the waterline at position x. The Wigley mathematical model with the same main dimensions as the experimental ship model was selected for the calculation, namely

$$S(x) = \frac{4bd}{3}\left[1 - \left(\frac{x}{L/2}\right)^2\right],$$

where b is half width of the ship, and d is the draft.

For a ship moving in channel, the sidewall condition is as follows:

$$\Phi_y = 0 \qquad \text{on} \quad y = -cw \quad \text{or} \quad (1-c)w \qquad (10)$$

where w is the width of channel, c is the ratio of the ship centre line away from right sidewall to the channel width, where $c = 1/2$ means the ship is moving along the channel centre line.

For a ship moving at subcritical speed, the governing equation is an elliptic equation. The upstream radiation condition is no wave before the ship, and the downstream radiation condition needs to be given.

For a ship moving at supercritical speed, the governing equation is a hyperbolic equation. The upstream radiation condition is also no wave before the ship, but the downstream radiation is the waves on downstream truncation boundary still move backward because of the limited calculation region.

Numerical Calculation Method

Without considering the change in the wetted hull surface, we used the finite difference method to calculate the SHPF motion at the symmetric centre line and off-centre, and we discretized the calculation region to a uniform rectangular grid. The x-direction along the ship length is marked with i, the upstream truncation boundary is at $i = 1$, and i increases downstream, in turn, with a grid spacing of Δx. The y-direction along the channel width is marked j, the right sidewall, $y = -cw$, is at $j = 1$, and j increases to the left sidewall in turn, with grid spacing of Δy.

For a ship moving at subcritical speed, according to its characteristic, the explicit-difference scheme is applied to the establishment of difference equations on discrete nodes. A three-node central-difference scheme of second-order preci-

sion is used for both Φ_{xx} and Φ_{yy}, and Φ_x and Φ_{xx} of the nonlinear term. For the dispersive term Φ_{xxxx}, a five-node partial upstream-difference scheme of first-order precision is used:

$$\left(\frac{\partial^4 \Phi}{\partial x^4}\right)_{i,j} = \frac{\Phi_{i+1,j} - 4\Phi_{i,j} + 6\Phi_{i-1,j} - 4\Phi_{i-2,j} + \Phi_{i-3,j}}{(\Delta x)^4} \qquad (11)$$

When a ship moves at subcritical speed, Equation (4) whose dispersion relation has been improved can be discretized as follows:

$$A\Phi_{i-3,j} + B\Phi_{i-2,j} + C\Phi_{i-1,j} + D\Phi_{i,j} + E\Phi_{i+1,j} = R_i \qquad (12)$$

where

$$A = 2\left(\frac{1}{3} + \beta\right)F_h^2 h^2 \Delta y^2,$$

$$B = -8\left(\frac{1}{3} + \beta\right)F_h^2 h^2 \Delta y^2,$$

$$C = 2(1 - F_h^2)\Delta x^2 \Delta y^2 + 12\left(\frac{1}{3} + \beta\right)F_h^2 h^2 \Delta y^2 - \frac{3V}{gh}\Delta x \Delta y^2 \Phi_{i-1,j},$$

$$D = -4(1 - F_h^2)\Delta x^2 \Delta y^2 - 4\Delta x^4 - 8\left(\frac{1}{3} + \beta\right)F_h^2 h^2 \Delta y^2$$
$$- \frac{6V}{gh}\Delta x \Delta y^2 \Phi_{i+1,j} + \frac{6V}{gh}\Delta x \Delta y^2 \Phi_{i-1,j},$$

$$E = 2\left(\frac{1}{3} + \beta\right)F_h^2 h^2 \Delta y^2 + 2(1 - F_h^2)\Delta x^2 \Delta y^2 + \frac{3V}{gh}\Delta x \Delta y^2 \Phi_{i+1,j},$$

$$R_i = -2\Delta x^4 (\Phi_{i,j-1} + \Phi_{i,j+1}).$$

If $\beta = 0$, it can be reduced to the discrete format of Equation (3), whose dispersion relation is not improved.

For a ship moving at supercritical speed, to reduce the numerical dissipation effect and ensure computational stability, the combination of a three-node central and upwind difference scheme was adopted for Φ_{xx} of the nonlinear term:

$$\left(\frac{\partial^2 \Phi}{\partial x^2}\right)_{i,j} = \frac{\alpha\Phi_{i+1,j} + (1-3\alpha)\Phi_{i,j} + (3\alpha-2)\Phi_{i-1,j} + (1-\alpha)\Phi_{i-2,j}}{(\Delta x)^2}$$
$$(13)$$

where α shows the proportion taken by the central difference scheme, with $0 \le \alpha \le 1$. For Φ_x of the nonlinear term, the three-node central-difference scheme was chosen for use (Liu and Chen, 2000). The difference scheme (Equation 11) was also used for the dispersive term Φ_{xxxx} of supercritical speed.

When a ship moves at supercritical speed, Equation (4), whose dispersion relation has been improved, can be discretized as follows

$$F\Phi_{i-3,j} + G\Phi_{i-2,j} + H\Phi_{i-1,j} + I\Phi_{i,j} + J\Phi_{i+1,j} = P_i \qquad (14)$$

where

$$F = 2\left(\frac{1}{3} + \beta\right)F_h^2 h^2 \Delta y^2,$$

$$G = 2(1 - F_h^2)\Delta x^2 \Delta y^2 - 8\left(\frac{1}{3} + \beta\right)F_h^2 h^2 \Delta y^2$$

$$+ \frac{3V}{gh}(1 - \alpha)(\Phi_{i+1,j})\Delta x \Delta y^2,$$

$$H = -4(1 - F_h^2)\Delta x^2 \Delta y^2 + 12\left(\frac{1}{3} + \beta\right)F_h^2 h^2 \Delta y^2$$

$$+ \frac{3V}{gh}(3\alpha - 2)(\Phi_{i+1,j} - \Phi_{i-1,j})\Delta x \Delta y^2,$$

$$I = 2(1 - F_h^2)\Delta x^2 \Delta y^2 - 8\left(\frac{1}{3} + \beta\right)F_h^2 h^2 \Delta y^2$$

$$- \frac{3V}{gh}(3\alpha - 1)(\Phi_{i+1,j} - \Phi_{i-1,j})\Delta x \Delta y,$$

$$J = 2\left(\frac{1}{3} + \beta\right)F_h^2 h^2 \Delta y^2 + \alpha\frac{3V}{gh}(\Phi_{i+1,j} - \Phi_{i-1,j})\Delta x \Delta y^2,$$

$$P_i = -2\Delta x^4 (\Phi_{i,j-1} + \Phi_{i,j+1}).$$

If $\beta = 0$, it can be reduced to the discrete format of Equation (3), whose dispersion relation is not improved.

When a ship moves at subcritical or supercritical speed, to ensure the stability of the computation of the nonlinear equation, very small, artificial, viscous terms of the type $v\Delta x^2 \Phi_{xxx}$ or $v\Delta y^2 \Phi_{yyy}$ need to be added to the upstream, downstream, and hull boundary conditions. The artificial viscous coefficient $v\Delta x^2$ and $v\Delta y^2$ are related to water depth, when $h = 0.2L$, and $v\Delta x^2$ and $v\Delta y^2$ are about 0.05 (Chen and SomDeo,1995; Demirdzic, Lilek, and Peric, 1993).

The disturbance velocity potential of the discrete node (i, j) can be solved with the iterative method, and the pressure coefficient can be expressed as follows

$$C_p = \frac{\Delta p}{0.5\rho V^2} = \frac{2}{V}\left(\frac{\partial \Phi}{\partial x}\right)_{i,j} = \frac{2}{V}\frac{(\Phi_{i+1,j} - \Phi_{i,j})}{\Delta x} \qquad (15)$$

where Δp refers to the variation in disturbance pressure of the water, and ρ is the density of the water.

To verify the proposed numerical calculation method and the improved mathematical model, we made a ship model that was 1 in nondimensional waterline length, 0.1979 in width, and 0.05208 in draught, and we developed an experimental system with high resolution and little error for the measurement of SHPF. The ship model was placed in the centre line of the towing tank with the following width: $w = 4.5L$, and it was towed by the trailer system at subcritical, transcritical, and supercritical speeds, respectively, so the experimental variation data in bottom pressure could be collected, reserved, and analyzed. The Wigley mathematical model, which is the same in the primary dimensions as the experimental ship model, was selected for the calculation (the details of the Wigley mathematical model and experimental ship model are shown in Figure 3; however, the former is different from the latter in stern shape, so we kept the bow position unchanged and increased the virtual ship length at the stern of Wigley mathematical model to make it correspond to the stern effects of the experimental ship (Deng *et al.*, 2013, 2014; Feng, 2008).

RESULTS

The typical results determined by numerical calculation and experiment are shown in Figures 4–7. Figure 4 shows that the improvement in dispersion relation and the proposed calculation method are correct, and the improved KP Equation (4) can yield better results. Figure 5 shows that the subcritical and supercritical SHPF in the off-centre motion of a different cw result and that $|C_{p_{\min}}|$ is greatly influenced when the cw is reduced. Figures 6 and 7 show that the narrower the distance between the ship and coastal sidewall, the greater is the SHPF effect on the coast. Figures 5–7 are the typical results of ship motion in the water area with different cw results, especially Figures 6c and 7b, which are the typical results of a ship sailing near the coast. Those results show that, when a ship is moving at subcritical speed, the narrower the distance between the ship and coastal sidewall, the greater will be the effects on the coast, the seabed, and the coastal architecture around the ship; meanwhile, when the ship moves at supercritical speeds, the narrower distance causes the effects on the coast, seabed, and coastal architecture of a much wider water and affects the coastal area behind the ship to a larger extent.

DISCUSSION

For a ship moving along the channel centre line, the finite-difference method was used to calculate the SHPF, based on Equation (3), whose dispersion relation is not improved and Equation (4) whose dispersion relation is improved, as shown in Figure 4. When $F_h = 0.55$, Figure 4a shows the longitudinal curve of SHPF of the subcritical speed calculated by Equation (4) is in better agreement with the experiment results than that calculated by Equation (3); moreover, the position and value of the negative-pressure coefficient peak calculated by Equation (4) are closer to the experimental results. When $F_h = 0.83$, Figure 4b shows that the position of negative and positive pressure coefficient peaks calculated by Equation (4) are much closer to the experimental results, especially the peak at the ship bow. When $F_h = 1.79$, Figure 4c shows that the longitudinal curve of SHPF at supercritical speeds, calculated by Equation (4), is also in better agreement with the experimental results. The peak position and the value calculated by Equation (4) conform to the experimental ones better than those calculated by Equation (3). Obviously, Equation (4), whose dispersion relation is improved, is suitable for a much wider range of speeds than is Equation (3), which is suitable for near-critical speeds. Meanwhile, the longitudinal curve of SHPF and the position of negative and positive pressure coefficient peaks calculated by Equation (4) are more accurate than those calculated by Equation (3). It is believed that the improvement of the dispersion relation and the proposed calculation method are correct, and the improved KP Equation (4) can yield better results; therefore, the following results are all calculated using the proposed calculation method based on the improved mathematical model (Equation 4). However, because we do not consider the change of a wetted hull surface, there is little difference between the calculated results and experimental ones, which we continue to research in the future.

Figure 5a shows a ship of $h = 0.2L$ and $w = 4.5L$ moving in the channel at subcritical speed $F_h = 0.52$. When $cw = 2.25L$ and the
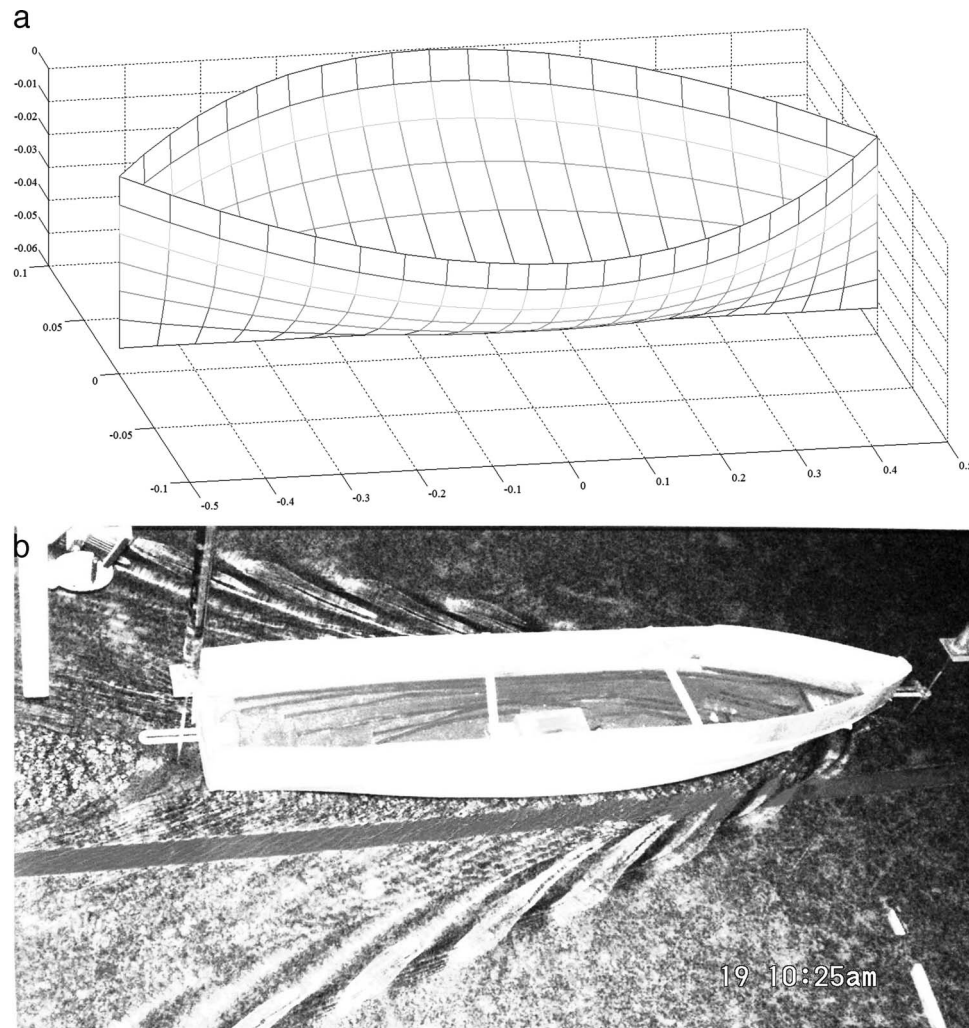
a

b

Figure 3. (a) The photo of the Wigley mathematical model. (b) The photo of the experimental ship model. Figure 3 helps us present the details of both ships.

ship moves along the channel centre line, the negative pressure coefficient peak $|C_{p_{\min}}|$ of SHPF is at a minimum, and it increases as the distance cw between the ship and right sidewall is reduced. When $cw < 1L$, with a reducing cw, the $|C_{p_{\min}}|$ increases more sharply, but the positive-pressure coefficient peak value decreases slowly, and the position of the peaks is unchanged. Figure 5b shows a ship of $h = 0.2L$ and $w = 4.5L$ moving in the channel at supercritical speed $F_h = 1.3$, with the cw reducing because of the superposition between the pressure variation of sidewall reflection and that of the moving ship; therefore, the negative-pressure coefficient peak $|C_{p_{\min}}|$ decreases instead of increasing, and the positive-pressure coefficient peak value near the stern of the ship increases and its position moves backward, but those near the bow of the ship are unchanged. Therefore, for a ship moving at subcritical speed, the peak position of the SHPF in the off-centre motion of various cw values remain unchanged, but $|C_{p_{\min}}|$ is greatly influenced as the cw is reduced. For a ship moving at supercritical speed, the positive-pressure coefficient peak near

the stern is obviously different than the off-centre motion of a different cw value, and the closer the ship is to the coast, the greater will be the coastal sidewall effect, and its position continues to move back, its value continues to decrease, and a much wider area of water behind the ship is influenced by the SHPF.

As shown in Figures 6 and 7, a ship of $h = 0.2L$ and $w = 4.5L$ is moving in the channel at transcritical speed $F_h = 0.9$. When the $cw = 2.25L$, the pressure variation on both sides of the ship is symmetrical, and the peaks of the SHPF occur on the channel or ship centre line. When the ship deviates from the channel centre line and moves near the coast, the peaks of SHPF move with the ship and still occur on the ship centre line. As the cw is reduced, the negative pressure coefficient peak $|C_{p_{\min}}|$ increases sharply because of the closer sidewall effect; meanwhile, the pressure variation around the ship fluctuates more drastically, and the pressure variation to the coast becomes more serious. The narrower the distance is between the ship and coastal sidewall, the greater will be the SHPF effect on the coast, which
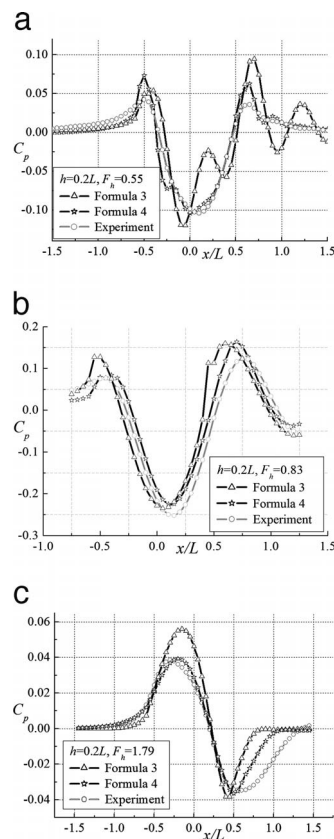
a

b

c

Figure 4. (a) When $w = 4.5L$, $cw = 2.25L$, $F_h = 0.55$, $h = 0.2L$, and $y = 0$, the longitudinal curves of pressure field were obtained separately by Equation (3), Equation (4), and the experiment. (b) When $w = 4.5L$, $cw = 2.25L$, $F_h = 0.83$, $h = 0.2L$, and $y = 0$, the longitudinal curves of pressure field were obtained separately by Equation (3), Equation (4), and the experiment. (c) When $w = 4.5L$, $cw = 2.25L$, $F_h = 1.79$, $h = 0.2L$, and $y = 0$, the longitudinal curves of pressure field were obtained separately by Equation (3), Equation (4), and the experiment. Figure 4a–c are typical results from the calculations and the experiment, and a comparison of the calculated results with the experimental ones shows that the SHPF characteristic calculated by the improved KP Equation (4) better approaches the experimental values. The calculations in Figures 5–7, therefore, were determined using Equation (4).

a

b

Figure 5. (a) When $w = 4.5L$, $F_h = 0.52$, $h = 0.2L$, and $y = 0$, the longitudinal curves of the pressure field of various cw values. (b) When $w = 4.5L$, $F_h = 1.3$, $h = 0.2L$, and $y = 0$, the longitudinal curves of the pressure field of various cw values.

improved and based on the model with the improved dispersion relation. The comparison of the calculated results with the experimental ones shows that the calculation method is feasible, and the mathematical model with an improved dispersion relation is more accurate and effective.

The finite-difference method was used to calculate the SHPF of various cw values, based on the mathematical model whose dispersion relation was improved, and we have presented the numerical calculation method for the SHPF caused by a ship deviating from the channel centre line or sailing near the coast.

The signal characteristic of the SHPF caused by a ship deviating from the channel centre line or sailing near the coast was obtained, and it indicates that when a ship moves at subcritical speeds, the narrower the distance is between the ship and the coastal sidewall, the greater will be the effects on the coast, the seabed, and the coastal architecture around the ship; moreover, when a ship is moving at supercritical speeds, the narrower the distance, the greater will be the effects on the coast, the seabed, and the coastal architecture because of the wider area of water behind the ship to a larger extent.

The bottom near a coast or in a channel may be uneven—one form of an unsteady effect—so we continue to research numerical methods of incorporating unsteady effects into the calculation of the SHPF.

results in a greater washing effect on the coast, the seabed, and coastal architecture around the ship.

CONCLUSIONS

Based on the shallow-water wave-potential flow theory and the assumption of a slender ship, a mathematical model was established for the pressure field caused by a moving ship, and a parameter was added in the coefficient for the dispersive term to improve its dispersion relation; therefore, we get an improved mathematical model, which is suitable for a wider range of speeds and can be used to obtain more-accurate SHPF characteristics.

The finite-difference method was used to calculate the pressure field caused by the ship moving at subcritical, transcritical, and supercritical speeds in shallow water, based on the mathematical model whose dispersion relation was not
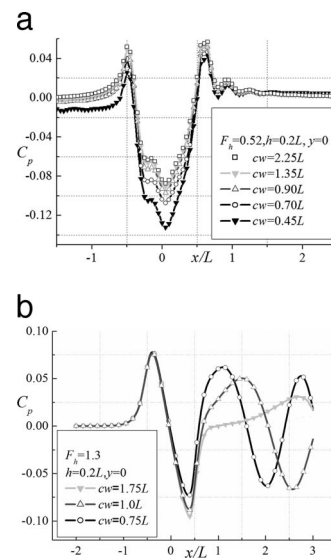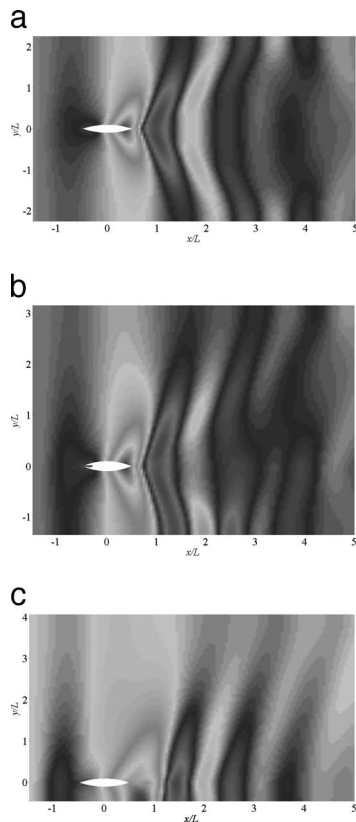
Figure 6. (a) When $w = 4.5L$, $h = 0.2L$, and $F_h = 0.9$, the two-dimensional distribution of SHPF for $cw = 2.25L$. (b) When $w = 4.5L$, $h = 0.2L$, and $F_h = 0.9$, the two-dimensional distribution of SHPF for $cw = 1.35L$. (c) When $w = 4.5L$, $h = 0.2L$, and $F_h = 0.9$, the two-dimensional distribution of SHPF for $cw = 0.45L$.
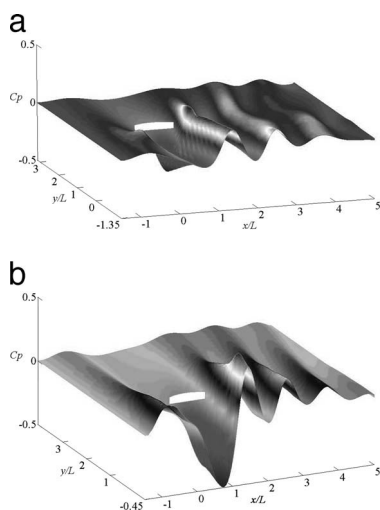

Figure 7. (a) When $w = 4.5L$, $h = 0.2L$, and $F_h = 0.9$, the three-dimensional distribution of SHPF for $cw = 1.35L$. (b) When $w = 4.5L$, $h = 0.2L$, and $F_h = 0.9$, the three-dimensional distribution of SHPF for $cw = 0.45L$.

LITERATURE CITED

Chen, X.N. and Sharma, S.D., 1995. A slender ship moving at a near-critical speed in a shallow channel. *Journal of Fluid Mechanics,* 291, 263–285.

Demirdžić, I.; Lilek, Z., and Perić, M., 1993. A collocated finite volume method for predicting flows at all speeds. *International Journal for Numerical Methods in Fluids,* 16, 1029–1050.

Deng, H.; Zhang, Z.H.; Gu, J.N., and Liu, J.B., 2013. Research on the calculation method of pressure field caused by the ship moving at subcritical speed in shallow water. *Applied Mathematics and Mechanics,* 34(8), 846–853.

Deng, H.; Zhang, Z.H.; Gu, J.N., and Liu, J.B., 2014. Numerical calculation and analysis of nonlinear pressure field induced by ship motion at subcritical speed in shallow water. *Ship Building of China,* 55(1), 11–19.

Feng, D.K., 2008. Computational Research on the Free Surface Flow Around Ship in Time Domain. Wuhan, China: Huazhong University of Science and Technology, Doctoral dissertation, 185p.

Jiang, T., 2001. *Ship Waves in Shallow Water*. Dusseldorf, Germany: Fortschritt-Berichte VDI. 138p.

Kozaczka, E. and Milanowski, L., 1995a. Experimental investigations of hydrodynamic pressure produced by a moving ship. *Proceedings of XII Symposium on Hydroacoustics* (Gdansk, Poland, ICA), pp. 10–16.

Kozaczka, E. and Milanowski, L., 1995b. *Elaboration of a Method for Determination of Ships' Hydrodynamic Field Distribution: Report on the Project "Hydrodynamic."* Gdynia, Poland: Gdynia Naval Academy, 43p.

Kozaczka, E. and Milanowski, L., 1997. Hydrodynamic pressure of a ship. *Proceedings of the International Symposium on Hydroacoustics and Ultrasonics* (Gdańsk, Poland, EAA), 15p.

Kozaczka, E.; Milanowski, L.; Komorowski, A., and Czarnecki, S., 1996. The application of the ship hydrodynamic field distribution for its localization. *Proceedings of the Undersea Defense Technology* (London, U.K., UDT), pp. 394–395.

Li, K.; Zhang, Z.H.; Gu, J.N., and Miao, T., 2011. Calculating pressure distribution on Water bottom caused by a moving ship with panel method. *Journal of Naval University of Engineering,* 23(1), 43–46.

Liu, J.B. and Chen, X.D., 2000. Pressure based method for 2-D transonic cascade flow. *Acta Aerodynamica Sinica,* 18(1), 105–110.

Miao, T.; Zhang, Z.H., and Gu, J.N., 2012. The calculation of ship wave and bottom pressure variation in finite depth by panel method. *Chinese Journal of Computational Mechanics*, 29(3), 464–469.

Sahin, I. and Hyman, M.C., 1993. Numerical calculation of the flow of submerged bodies under a free surface. *Ocean Engineering,* 20(3), 339–345.

Sahin, I.; Crane, J.W., and Watson, K.P., 1997. Application of a singularity panel method for hydrodynamics of underwater vehicles. *Ocean Engineering,* 24(6), 501–512.

Sahin, I.; Hyman, M.C., and Nguyen, T.C., 1994. Three-dimensional flow around a submerged body in finite-depth water. *Applied Mathematical Modeling,* 18(11), 611–619.

Tuck, E.O., 1966. Shallow water flows past slender bodies. *Journal of Fluid Mechanics,* 26(1), 81–95.

Tuck, E.O., 1978. Hydrodynamic problems of ships in restricted waters. *Annual Review of Fluid Mechanics,* 10, 33–46.

Tuck, E.O., 1998. *Bottom Pressure Signatures*. Adelaide, Australia: University of Adelaide, 35p.

Zhang, Z.H., 2003. Investigation and Engineering Application of Hydrodynamic Pressure Field Caused by Ship Moving at Subcritical and Supercritical Speed. Wuhan, China: Naval University of Engineering, Doctoral dissertation, 181p.

Zhang, Z.H. and Gu, J.N., 2006. Research on wave and pressure field caused by ship moving at high speed in shallow water. *Journal of Ship Mechanics*, 10(2), 15–22.

Zhang, Z.H.; Gu, J.N.; Zheng, X.L., and Gong, S.G., 2002a. Pressure variation on shallow water bottom caused by moving ship. *Ship Building of China,* 2, 9–14.

Zhang, Z.H.; Gu, J.N.; Zheng, X.L., and Gong, S.G., 2002b. Experimental study of Hydrodynamic pressure field caused by a moving ship in finite-water. *Journal of Hydrodynamics,* 6, 9–14.

Zheng, C.W. and Li, C.Y., 2015. Variation of the wave energy and significant wave height in the China Sea and adjacent waters. *Renewable and Sustainable Energy Reviews,* 43, 381–387.

Zheng, C.W.; Zhou, L.; Jia, B.K.; Pan, J., and Li, X., 2014. Wave characteristic analysis and wave energy resource evaluation in the China Sea. *Journal of Renewable and Sustainable Energy,* 6, 043101.

Zhou, H.X. and Zhen, B.Y., 2006. Discussion on defining deep water, shallow water and restricted channel. *Port and Waterway Engineering,* 384(1), 53–58.